

SESAM and T χ L Results for Wilson Action–A Status Report

Th. Lippert^{a*}, G. Bali^b, N. Eicker^a, L. Giusti^c, U. Glässner^d, S. Güsken^d, H. Hoerber^d, P. Lacock^a, G. Martinelli^c, F. Rapuano^c, G. Ritzenhöfer^a, K. Schilling^{a,d}, G. Siegert^a, A. Spitz^a, P. Ueberholz^d, and J. Viehoff^d

^aHLRZ, c/o Jülich Research Center and DESY, Hamburg, D-52425-Jülich, Germany

^bPhysics Department, The University, Southampton SO17 1JB, UK

^cINFN, University “La Sapienza”, P’lle Aldo Moro, Roma, Italy

^dDepartment of Physics, University of Wuppertal, D-42097 Wuppertal, Germany

Results from two studies of full QCD with two flavours of dynamical Wilson fermions are presented. At $\beta = 5.6$, the region $0.83 > \frac{m_\pi}{m_\rho} > 0.56$ at $m_\pi a > (0.23L)^{-1}$ is explored. The SESAM collaboration has generated ensembles of about 200 statistically independent configurations on a $16^3 \times 32$ -lattice at three different κ -values and is entering the final phase of data analysis. The T χ L simulation on a $24^3 \times 40$ -lattice at two κ -values has reached half statistics and data analysis has started recently, hence most results presented here are preliminary. The focus of this report is threefold: (i) we demonstrate that algorithmic improvements like fast Krylov solvers and parallel preconditioning recently introduced can be put into practise in full QCD simulations, (ii) we present encouraging observations as to the critical dynamics of the Hybrid Monte Carlo algorithm in the approach to the chiral limit, (iii) we mention signal improvements of noisy estimator techniques for disconnected diagrams to the π - N σ term, and (iv) we report on SESAM’s results for light hadron spectrum, light quark masses, and heavy quarkonia.

1. INTRODUCTION

In this talk I will give an interim status report about two large-scale computer simulations of full lattice QCD with two degenerate flavours of dynamical Wilson fermions. Both simulations, SESAM and T χ L, are based on the Hybrid Monte Carlo algorithm [1,2] at an inverse coupling of $\beta = \frac{6}{g^2} = 5.6$, running on $16^3 \times 32$ and $24^3 \times 40$ lattices, respectively. Our platform is the parallel supercomputer APE100/Quadrics. The SESAM simulation took place on a 256-node 12.8 Gflops machine, while the T χ L production is still ongoing on two 512-node 25.6 Gflops system. Our goal is to reveal the effects of dynamical quarks on physical quantities, hence we operate as close as possible to the chiral limit. It goes without saying that this task requires large lattices and high statistics. Therefore both *technical* and *algorithmic* improvements are crucial to achieve the

progress needed. As we Europeans are still living in the Pre-Teraflops era, we have put much emphasis on the *improvement* of numerical algorithms and the verification of their *stochastic efficiency*. I will show in this contribution that we (i) could boost our simulation speed substantially and (ii) perform a reliable determination of the autocorrelation time τ of the HMC algorithm. Another important issue of our work is signal preparation in the computation of disconnected diagrams to the π - N σ term. The last part of my talk is devoted to physics results on light hadron and quark masses and heavy quarkonia.

1.1. SESAM

The name ‘SESAM’ is our slogan and magic acronym in the search for **Sea Quark Effects on Spectrum And Matrix Elements** in full QCD with dynamical Wilson fermions. This is indeed a Tera-computing task. In order to meet the challenge within the resources available to us

*Presented by Th. Lippert

we decided to head for a landmark by aiming at high statistics at *one* value of β rather than attempting a full scaling investigation [3]. Needless to say that, with Pre-Teraflops machines, it is highly non-trivial to position the hopping parameter window for the observation of sea quark effects.

The sea-quark masses and lattice resolutions in the SESAM simulation were chosen as small as possible in order to be sensitive to sea-quark effects and not be disturbed by scaling violations. Based on experience from quenched simulations we aimed at lattice spacings of $a \approx 0.1$ fm corresponding to the quenched $\beta \approx 6.0$ in order to make contact to the scaling region. The results of the SCRI-group on the full-QCD β -function [4] suggested to go beyond $\beta = 5.5$ in order to escape the strong coupling regime. To end up with a reasonable physical lattice size—from valence quark studies at all three different κ_{sea} 's—we chose to work at $\beta = 5.6$.

In the tuning of κ towards its chiral regime, we aim at small values of m_π/m_ρ , under the condition that finite-size effects remain tolerable. In fact we required $m_\pi a L \geq 4$. This limits the smallest $\frac{m_\pi}{m_\rho}$ ratio that can be attained. We approached this minimal $\frac{m_\pi}{m_\rho}$ in an iterative manner, starting with our largest bare mass. We took into account the statistics that could be achieved given 1 year runtime on a 256 node Quadrics QH2, extrapolating the algorithmic specifications from [3,5]. Eventually we have generated ensembles at 3 dynamical κ -values, $\kappa_{\text{sea}} = 0.1560, 0.1570$ and 0.1575 . Production ended in December 1996. Altogether, for the SESAM project, we have spent on APE slightly more than 100 Teraflops-hours. In order to put the statistics achieved with APE into perspective we present an overview of the characteristics of recent full QCD simulations with dynamical Wilson fermions in Tab. 1 and in Fig. 1.

The SESAM run parameters together with some major monitoring quantities are given in Tab. 2. The average number of iterations is denoted by $\# \text{ it}$, while N_{md} stands for the number of molecular dynamics steps for a trajectory, which varies stochastically according to a symmetric distribu-

of HMC trajectories

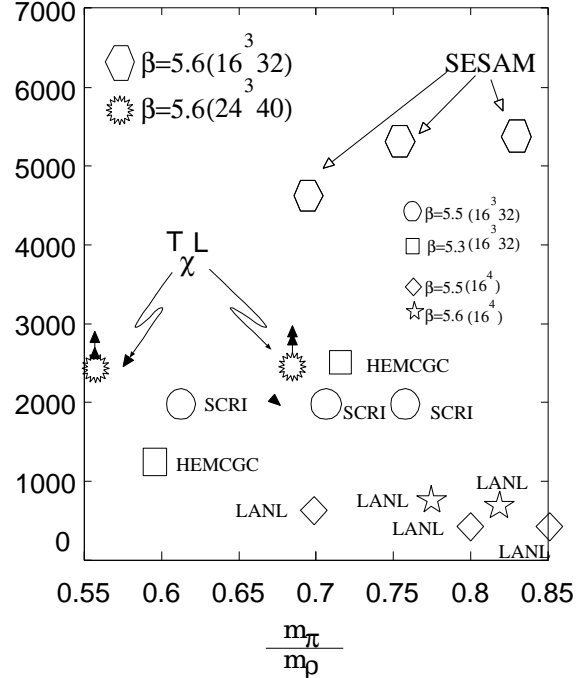


Figure 1. SESAM and $T\chi L$ statistics as a function of the control parameter m_π/m_ρ , compared to preceding full QCD simulations with Wilson fermions.

tion of width σ in order to avoid interlocks with Fourier modes. $r = \frac{|Mx - \phi|}{|x|}$ is the stopping criterion for the iterative solver, alg specifies the inversion algorithm used, see sections 2.1. and 2.2. After thermalization of each κ -run we have held the molecular dynamics parameters fixed; this enables us to carry out a sensible autocorrelation analysis. We found that switching κ , while holding the molecular dynamics time step fixed, is affecting the acceptance rate only marginally, see Tab. 2. Therefore we have used a universal time step of $dt = 0.01$ for most dynamical samples.

It was one of the goals of SESAM to perform for the first time a detailed autocorrelation study on an adequate set of physical quantities. To

Table 1

Some characteristic figures from SESAM, T χ L and previously performed large scale simulations with two flavours of dynamical Wilson fermions.

group	size	β	κ	L_S [fm]	L_{traj}	machine
SESAM	$16^3 32$	5.6	0.156	1.44(5)	5400	QH2
			0.157	1.39(4)	5350	
			0.1575	1.32(4)	4500	
T χ L	$24^3 40$	5.6	0.1575	1.93	2500	QH4
			0.1580		2400	
LANL[3]	16^4	5.4	0.1600	2.16	564	CM2
			0.1610		972	
			0.1620		239	
		5.5	0.1580	1.664	301	CM2
			0.1590		396	
			0.1600		514	
		5.6	0.1560	1.232	601	CM2
			0.1570		756	
	$16^3 32$	5.5	0.1600		231	CM2
		5.6	0.1570		318	CM2
			0.1575		168	
HEMCGC[5]	$16^3 32$	5.3	0.1670	1.744	2425	CM2
			0.1575		1270	
SCRI[6]	$16^3 32$	5.5	0.1596		~ 2000	CM2
			0.1600		~ 2000	
			0.1604		~ 2000	

this end we decided to archive all HMC trajectories and study more difficult observables, such as glueballs and topological features, in postprocessing style using the Crays T3E, T90 and Personal Computers at HLRZ Jülich.

Simulations of full QCD with two flavours of Wilson fermions at zero temperature so far have been carried out on lattices of size $\leq 16^3 \times 32$ and ratios of $\frac{m_\pi}{m_\rho} > 0.6$ [3,5–7]. The results of SESAM demonstrate that dedicated supercomputers in the range of about 10 Gflops performance can indeed generate in one year’s runtime statistically significant full QCD samples at $\frac{m_{PS}}{m_V} \simeq 0.70$. Alas, according to χ PT (constructing a fictitious pseudoscalar meson containing two ‘strange quarks’, with mass ratio of the size quoted),

$$\frac{m_{ps}}{m_\phi} \approx \frac{\sqrt{2m_K^2}}{m_\phi} = 0.69, \quad (1)$$

we find ourselves still in the region of strange quarks. Thus, in order to quantify light sea quark effects in full QCD, one would wish to come closer to the chiral limit and to finer lattice resolutions than achieved previously. This implies larger lattice volumes.

1.2. T χ L

In a feasibility study on a $24^3 \times 40$ lattice we have investigated whether a further step towards the chiral limit is in reach of the APE Tower computing power. We tuned ourselves to a realistic working point at a volume of $(2 \text{ fm})^3$, with chirality characterised by $\frac{1}{m_{\pi a}} \approx 5.6$ and $\frac{m_\pi}{m_\rho} < 0.6$ [8]. We found that by use of preconditioning techniques we could accelerate the matrix inversion [9,10] sufficiently for a 512-node APE Tower to drive an optimised HMC code fast enough (*i*) to increase the lattice size by more than a factor of 4 compared to the previous standards including

Table 2

Simulation parameters and some monitor quantities for the SESAM runs.

κ	alg	T	$N_{md} \pm \sigma_{N_{md}}$	acc [%]	r	# it	N_{CSG}	$\frac{m_\pi}{m_\rho}$	# traj	# therm
0.156	o/e	1	100 ± 20	85	10^{-8}	85(3)	6	0.8388(41)	5000	400
0.1570	o/e	1	100 ± 20	84	10^{-8}	168(5)	8	0.7552(69)	3500	350
	SSOR	1	100 ± 20	80	10^{-8}	125(3)	9		1500	0
0.1575	o/e	1	100 ± 20	76	10^{-8}	317(12)	11	0.688(12)	3000	500
	SSOR	0.5	71 ± 12	73	10^{-8}	150(6)	3		2000	0

SESAM, (ii) and to go more chiral.

In the framework of the Italian-German $T\chi L$ -collaboration we launched an 18 month Hybrid Monte Carlo simulation, mainly running on the APE100 Tower at INFN Rome and partly on the QH4 Zeuthen/Berlin at $\beta = 5.6$. Our HMC implementation reaches a sustained performance of 17 Gflops with 25.6 Gflops being the APE Tower peak speed.

We switched from the thinned o/e representation to the full representation of the fermionic matrix $M = \mathbf{1} - \kappa D$, employing our new SSOR preconditioning scheme, see section 2.2. On the APE machine, this scheme offers about an overall gain of a factor of 2 in machine time, see Tab. 3.

We have chosen two κ -values, 0.1575 and 0.158 for two reasons: (i) $\kappa = 0.1575$ coincides with the smallest mass value of the SESAM project relating the two lattice sizes at a definite point in parameter space. Thus we are able to assess both the influence of finite size effects on physical quantities and the volume dependence of the simulation algorithm. (ii) The $24^3 \times 40$ lattice allows to increase the pion correlation length in lattice units, ξ_π , by a factor of 1.5 compared to the smallest dynamical mass of the SESAM project, which we estimated to be sufficient for a chirality $\frac{m_\pi}{m_\rho}$ in the range of .55. As the lattice scale is refined when reducing the bare quark masses we decided to stay with $\beta = 5.6$.

In order to perform a scaling analysis it would have been desirable to simulate at different β -values. The peephole to scaling, *cf.* Fig. 2, discloses unfortunately that a substantial decrease in scale a would be needed in order to have a sufficient lever arm in the continuum extrapolation.

It is instructive though to compare Fig. 2 to recent improved action results [11].

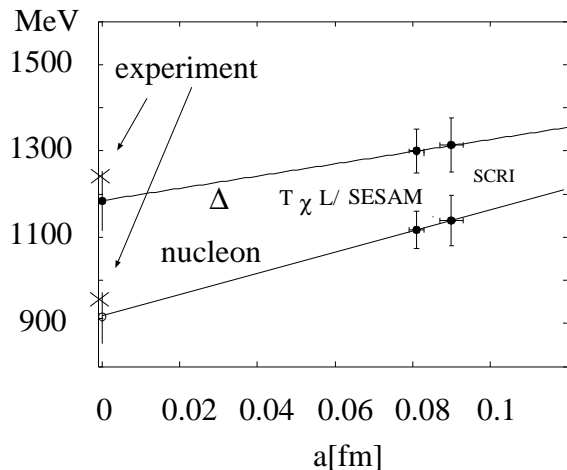


Figure 2. “Continuum extrapolation” for baryon masses (together with SCRI data [6]) obtained at $\beta = 5.5$.

During the layout phase of $T\chi L$ (Feb. 1996) we determined the most chiral κ_{sea} value extrapolating the relation $m_q a = \frac{1}{2} \left(\frac{1}{\kappa} - \frac{1}{\kappa_{sea}^c} \right)$ on the SESAM data available at the time. Requiring $\frac{\xi_\pi}{24a} = .23$ we arrived at $m_q a = 0.023$ corresponding to $\kappa = 0.1580$, *cf.* Fig. 3. We considered this value of ξ_π as small enough not to suffer from large finite size effects. Needless to say: at the end of the day it remains to be seen, see section

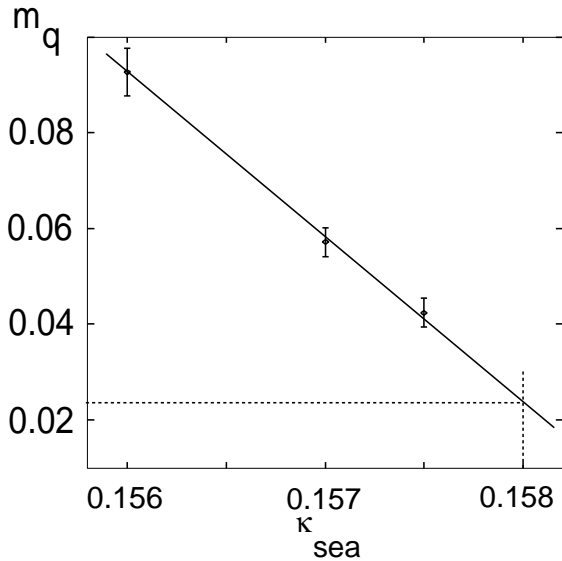


Figure 3. Fixing κ_{sea} for $T\chi L$ from SESAM data.

5, that this parameter choice is reasonably positioned within the ‘chirality gap’. At the time of this meeting, we have generated two ensembles of configurations at $\kappa = 0.1575$ and $\kappa = 0.158$, with more than 2400 trajectories each, within 150 Teraflops-hours. For $T\chi L$ we were not able to archive each trajectory so we decided to store every other for later autocorrelation analysis and detailed postprocessing.

The $T\chi L$ run parameters and some monitoring quantities of interest are collected in Tab. 3. t specifies the time to generate one trajectory on the APE Tower.

2. OPTIMIZING HMC

The optimisation of fermionic simulation algorithms constitutes a major target of the scientific program of the Wuppertal-HLRZ lattice QCD group. From the beginning the two projects, SESAM and $T\chi L$, have been accompanied by algorithmic research in collaboration with the Applied Mathematics group at Wuppertal University. We have focused on the acceleration of Krylov sub-

space solvers within the computer intensive inversion part of HMC that is required to calculate the fermionic force [12,13]. In these studies the so-called biconjugate gradient stabilised method (BiCGstab) has been established as the most efficient Krylov solver for Wilson fermion matrix inversions. It behaves quasi-optimal, *i.e.*, it approaches the convergence speed of GMRES, the (non-practical) optimal reference Krylov solver. Therefore, to make further progress, one has to address the development of new parallel preconditioning methods [9,14].

2.1. Krylov solvers

The practical iterative methods to solve the huge system of equations $MX = \phi$ belong to the class of Krylov subspace methods. In the old days the minimum residual algorithm (MR) has been established as *the* efficient method for both propagator computations and the calculation of the fermionic force within the HMC [15]. In the early nineties, numerical analysts were successful in developing new Krylov subspace methods [16,17]. These methods avoid the squared condition number (from $M^\dagger M$ inversion) of CG, and yet guarantee convergence as opposed to MR.

In Refs. [12,13,18] we have benchmarked and improved various iterative solvers (within simplified settings) in order to find the fastest solver for Wilson fermion matrix inversions.

Using SESAM’s configurations we can confirm the findings of [12]. The over-relaxed MR algorithm outperforms CG, however BiCGstab beats ORMR, see Fig. 2.1. This behaviour is qualitatively the same for all three κ_{sea} -values used by SESAM.

Comparing the convergence behaviour of BiCGstab with that of OrthoMin(N) reveals that BiCGstab is close to the optimal algorithm GMRES. GMRES orthonormalises on all previous search directions and therefore is not practical. OrthoMin(N) [19] is a practical modification of the latter, orthogonalising on N previous directions only. The insertion demonstrates that BiCGstab is beating OrthoMin up to a depth of $N = 10$ and further on is about 10 % less efficient in terms of iterations. In view of these findings,

Table 3
Simulation parameters and some monitor quantities for the T χ L runs.

κ	alg	T	$N_{md} \pm \sigma_{N_{md}}$	r	t/traj [s]	$\frac{m_\pi}{m_\rho}$ [prel!]	# traj	# therm
0.1575	o/e	1	125 ± 20	10^{-8}	8200			
	SSOR	0.5	125 ± 20	10^{-8}	3800	0.70(4)	2500	500
0.158	SSOR	0.5	125 ± 20	10^{-8}	9200	0.56(4)	2400	800

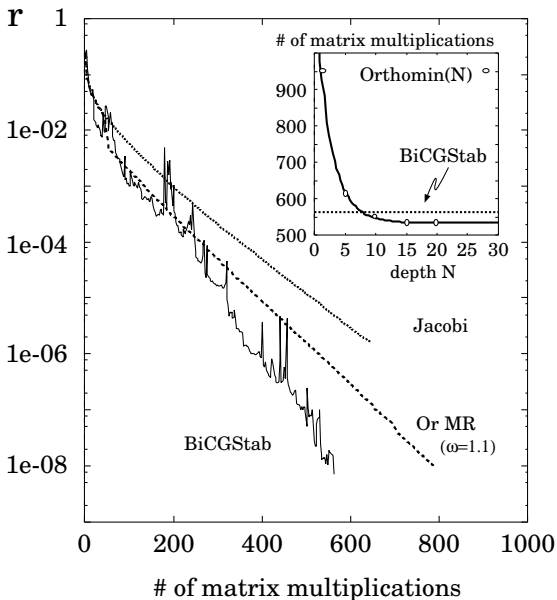


Figure 4. Comparing the convergence of the simple Jacobi iteration, ORMR and BiCGstab at $\beta = 5.6$ and $\kappa = 0.1575$ for a typical $16^3 \times 32$ full QCD configuration. The insertion shows the results for OrthoMin(N) compared to BiCGstab (straight line).

BiCGstab can be considered as *quasi optimal*².

2.2. Parallel preconditioning

The quasi-optimality of BiCGstab suggests to turn attention on multigrid methods and/or preconditioning in order to achieve further speed up in Wilson fermion matrix inversions. The applica-

²In terms of computer time expense, BiCHstab is more efficient.

tion of multigrid techniques is impractical, however, due to the gauge noise of the gluonic background field entering the fermion matrix. Thus preconditioning techniques, *i.e.* methods to decrease the condition number K^2 of $M^\dagger M$ appear to be the only promising path to further accelerate Krylov subspace solvers like BiCGstab.

A standard preconditioning approach in lattice gauge computations rests upon o/e decomposition of M [20]. It can yield an efficiency gain by a factor of 2 when inverting M . Some years ago, Oyanagi [21] exploited incomplete LU (ILU) factorisation of the matrix M based on the natural, *globally lexicographic* ordering of the lattice points³. On local memory or grid-oriented parallel computers, this preconditioner can hardly be implemented efficiently, however.

Recently we have introduced a new parallel preconditioning technique suitable for Wilson fermion matrix inversions. Our method is called *local lexicographic SSOR preconditioner* (LL-SSOR). As opposed to familiar multicolour SSOR preconditioners (like the o/e preconditioner) which produce a decoupling of variables on a very fine grain level, the LL-SSOR method provides the flexibility to reduce the decoupling to the minimum which is necessary to suit a given parallel system. As for any SSOR preconditioner, the Eisenstat Trick [22] is crucial for the efficient implementation of LL-SSOR. Our numerical experiences show that LL-SSOR presently offers the fastest available solution method on parallel computers.

The general preconditioning of M proceeds via two non-singular matrices V_1 and V_2 , the left and

³For the Wilson fermion discretisation with Wilson parameter $r = 1$, ILU preconditioning is identical to symmetric successive over-relaxation (SSOR) preconditioning with respect to that ordering.

right preconditioners, respectively:

$$\begin{aligned} V_1^{-1} M V_2^{-1} \tilde{x} &= \tilde{\phi}, \\ \text{where } \tilde{\phi} &= V_1^{-1} \phi, \tilde{x} = V_2 x. \end{aligned} \quad (2)$$

A Krylov solver could now be applied directly, by replacement of each occurrence of M and ϕ by $V_1^{-1} M V_2^{-1}$ and $\tilde{\phi}$.

We have chosen to apply symmetric Gauß-Seidel (SSOR) preconditioning. The matrix M has to be decomposed into its diagonal, strictly lower and strictly upper triangular parts, $M = I - L - U$. Then the SSOR preconditioner is specified by

$$V_1 = I - L, \quad V_2 = I - U. \quad (3)$$

Now we find that $V_1 + V_2 - M = I$. This relation allows to exploit the Eisenstat-trick [22]: $V_1^{-1} M V_2^{-1} = V_2^{-1} + V_1^{-1}(I - V_2^{-1})$, so that the matrix vector product $w = V_1^{-1} M V_2^{-1} r$ amounts to a 2-step computation

$$v = V_2^{-1} r, \quad u = V_1^{-1}(r - v), \quad w = v + u. \quad (4)$$

The general preconditioned BiCGstab procedure is described in Ref. [9].

Since the matrices $I - L$ and $I - U$ are triangular, their inversions are simply performed by *forward* and *backward* substitution, respectively. As example the forward solve $(I - L)y = p$ becomes:

$$\text{for } i = 1, \dots, n \\ (y)_i = (p)_i + \sum_{j=1}^{i-1} (L)_{ij} (y)_j.$$

In terms of computational cost, a forward followed by a backward solve is as expensive as a multiplication with M . Hence in principle there is no increase of computational cost with SSOR.

In the solution of the Wilson fermion inversion problem the ordering scheme for the lattice points x is completely arbitrary. Different orderings yield different matrices M , permutationally similar to each other. The efficiency of the SSOR preconditioner depends on the ordering scheme chosen.

Consider an arbitrary numbering (ordering) of the lattice points. For a given grid point x , the corresponding row in the matrix L or U contains exactly the coupling coefficients of those nearest neighbours of x which have been numbered before or after x , resp. Therefore, a generic formulation of the forward solve for this ordering is given by Algorithm 1. The backward solves are done similarly, now running through the grid points in *reverse* order.

Algorithm 1 Forward Solve.

```

for all grid points  $x$  in the given order
{ update  $y_x$  }
 $y_x = p_x$ 
for  $\mu = 1, \dots, 4$ 
  if  $x - \mu$  was numbered before  $x$  then
     $y_x = y_x + \kappa \cdot m_{x, x-\mu}^+ y_{x-\mu}$ 
for  $\mu = 1, \dots, 4$ 
  if  $x + \mu$  was numbered before  $x$  then
     $y_x = y_x + \kappa \cdot m_{x, x+\mu}^- y_{x+\mu}$ 

```

So far, odd-even preconditioning was considered as the only successful preconditioner for lattice QCD that is parallelisable. For this particular ordering the inverses of $I - L$ and $I - U$ can be determined directly, see Ref. [9].

Oyanagi some time ago [21] has demonstrated that ILU (SSOR) preconditioning, applying global lexicographic ordering, yields an improvement over odd-even preconditioning as far as the number of iterations is concerned. However, its parallel implementation is difficult [23].

The ordering we have proposed is similar to Oyanagi's approach, however, it is intrinsically parallelisable, and it is adaptive to the parallel computer used. We assume that the processors of the parallel computer are connected as a $p_1 \times p_2 \times p_3 \times p_4$ 4-dimensional grid. The space-time lattice can be matched to the processor grid in an obvious natural manner, producing a local lattice of size $n_1^{loc} \times n_2^{loc} \times n_3^{loc} \times n_4^{loc}$ with $n_i^{loc} = n_i/p_i$ on each processor.

The whole lattice is divided into $n^{loc} = n_1^{loc} n_2^{loc} n_3^{loc} n_4^{loc}$ groups. Each group corresponds to a fixed position of a site in the local grid. Associating a colour with each of the groups, we can interpret this process as a colouring of the lattice points, see Fig. 5.

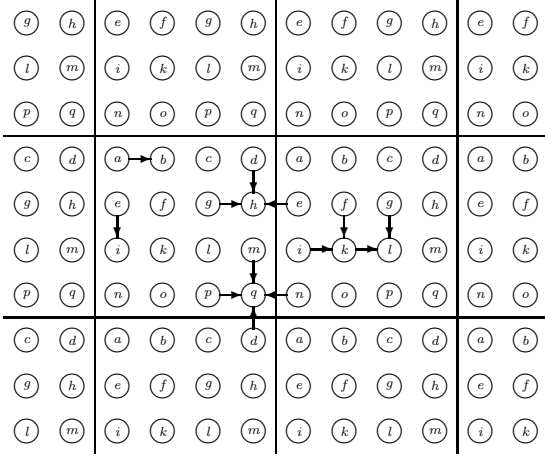


Figure 5. Locally lexicographic ordering and forward solve in 2 dimensions.

All nearest neighbours of a given grid point have colours different from that point. Performing the forward and backward solves within the BiCGstab algorithm, grid points having the same colour can be worked upon in parallel, thus yielding an optimal parallelism of p , the number of processors.

A formulation of the ll -forward solve is given in Algorithm 2. Here, we use ‘ \leq_{ll} ’ as a symbol for ‘ ll -less than’.

On the ‘local boundaries’ we will have between 0 (for the ll -first point) and 8 (for the ll -last point) summands to add to p_x . The parallelism achieved is p , and thus is optimal since we have p processors. If we change the number of processors, the ll -ordering, and consequently the properties of the corresponding SSOR preconditioner will change, too.

The efficiency of LL-SSOR has been tested in the framework of SESAM and T χ L simulations. First we display performance results for $\kappa = 0.157$ on an $8^3 \times 16$ lattice at $\beta = 5.6$. In Fig. 6 we show that the convergence speed of LL-SSOR is about twice as fast as that of o/e preconditioning and nearly reaches that of Oyanagi preconditioning.

On Quadrics we have achieved a *real overall speed up* of a factor between 1.5 and 2.1 compared to our o/e implementation, see Tab. 3; however, this is a machine dependent result.

Algorithm 2 ll -forward.

for all colours in lexicographic order
 for all processors
 $x :=$ grid point of that colour on that processor
 { update y_x }

$$y_x = p_x + \kappa \left(\sum_{\mu, x-\mu \leq_{ll} x} m_{x, x-\mu}^+ y_{x-\mu} + \sum_{\mu, x+\mu \leq_{ll} x} m_{x, x+\mu}^- y_{x+\mu} \right)$$

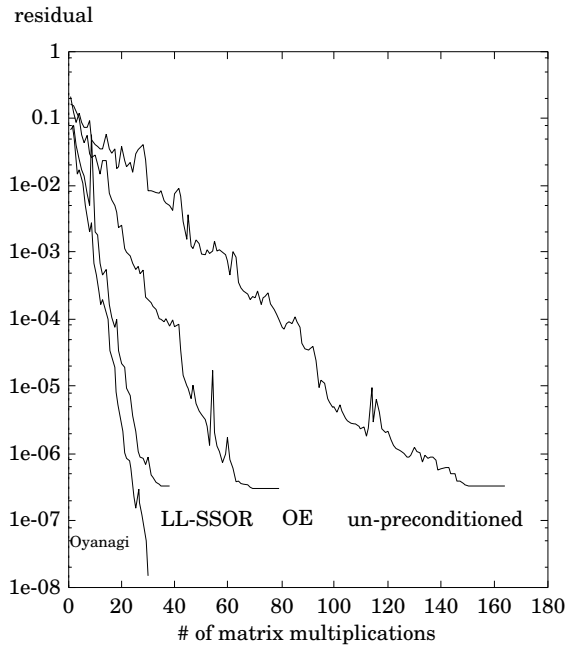


Figure 6. Residue reached by a given number of matrix-multiplications.

We also can present results for the volume dependency of the LL-SSOR preconditioning, see Fig. 7.

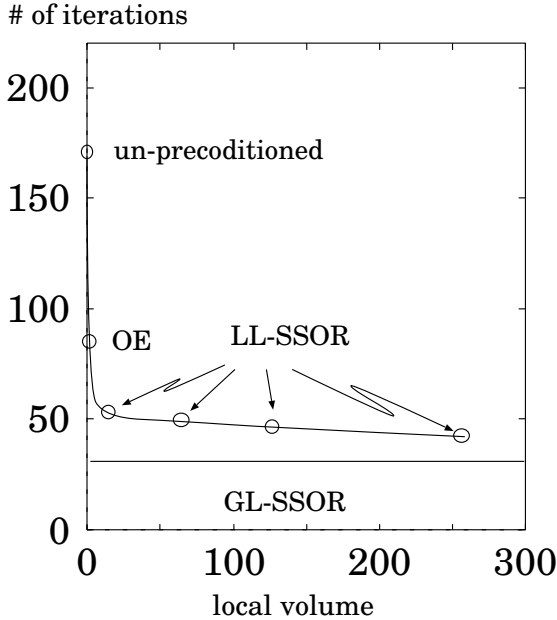


Figure 7. Volume dependency of LL-SSOR efficiency for BiCGstab.

Finally we remark that preconditioning and chronological start vector guess (CSG) [24] as applied in the molecular dynamics evolution part of HMC are nearly additive in their iteration gain.

3. CRITICAL DYNAMICS

The HMC algorithm is a Markov process at heart. Therefore, a full QCD vacuum configuration series exhibits autocorrelation. Its statistical quality is affected crucially by this autocorrelation which depends in general on the physical observable under investigation and are increasing in the approach to the chiral limit.

The exact determination of the autocorrelation function amounts to trace the system over infinite time. Any practical Markov process is finite, however, and it is so much the worse that t_{MC} in full QCD Hybrid Monte Carlo simulations is not large enough compared to the relaxation time, $t_{MC} \simeq \tau_{exp}$. So far this has prevented a

reliable determination of autocorrelations in full QCD simulations with Wilson fermions.

SESAM has increased the trajectory samples by nearly one order of magnitude compared to previous studies⁴. It is important to note that we rested under stable conditions for the HMC dynamics to evolve rather than retuning MD parameters as production went on. This provides the setting for a reliable determination of autocorrelation times related to various gluonic and hadronic quantities.

Given a time-series of measurements A_t , $t = 1, \dots, t_{MC}$ we compute a finite time-series approximation to the true autocorrelation function for observable A :

$$C^A(t) = \frac{1}{t_{MC} - t} \sum_{s=1}^{t_{MC}-t} A_s A_{s+t} - \left(\frac{1}{t_{MC} - t} \sum_{s=1}^{t_{MC}} A_s \right)^2. \quad (5)$$

This two-point function in the Monte Carlo time can be normalised by

$$\rho^A(t) = \frac{C^A(t)}{C^A(0)}. \quad (6)$$

The *exponential* autocorrelation time is defined as the inverse decay rate of the slowest mode contributing to the autocorrelation function:

$$\tau_{exp}^A = \limsup_{t \rightarrow \infty} \frac{t}{-\log \rho^A(t)}. \quad (7)$$

τ_{exp}^A is a relaxation parameter and is related to the length of the thermalization phase [25] of the Markov process. In our simulations we required the thermalization length to be $5 \times \tau_{exp}$ such as to achieve a suppression of the starting conditions of order $\mathcal{O}(\exp(-5))$ in the ensemble. Furthermore τ_{exp}^A is a characteristic time to achieve ergodicity: the simulation has to be much larger than $\sup_A \{\tau_{exp}^A\}$.

The *integrated* autocorrelation time is defined as the integral:

$$\tau_{int}^A = \frac{1}{2} + \sum_{t'=1}^{t_{MC} \rightarrow \infty} \rho^A(t'). \quad (8)$$

⁴T χ L aims at $O(4000)$ trajectories per dynamical sample.

In equilibrium τ_{int}^A characterises the true statistical error of the observable A computed from the ensemble. The sample mean

$$\langle A \rangle = \frac{1}{N} \sum_{i=1}^N A(i), \quad (9)$$

has the variance

$$\sigma_A^2 \approx \frac{1}{N-1} 2\tau_{int}^A C^A(0) = 2\tau_{int}^A \sigma_0^2, \quad (10)$$

for $N \gg \tau_{int}^A$,

which is increased by the factor $2\tau_{int}^A$ compared to the result over a sample of N independent configurations. In our simulations, configurations separated by 2 to $3 \times \tau_{int}^A$ are considered as ‘decorrelated’⁵.

On a finite time-series it is difficult to estimate the slowest exponential autocorrelation time reliably as the tail of the autocorrelation function becomes compatible with zero. This leads to an unwanted bias in τ_{int}^A . A practical solution to this problem is the application of a ‘window’ procedure as introduced in Ref. [25] to extract the integrated autocorrelation time: a cut-off t in the sum for τ_{int}^A is increased until a plateau becomes visible. As a rule of thumb, it has been suggested in [25] to determine t self-consistently in the range 4 to $10\tau_{int}^A$. This amounts to a truncation effect (difference to the true τ_{int}) of less than 2%.

The integrated autocorrelation time τ_{int} can be observable dependent. One effect is due to the time-space extension of lattice observables. Very extended quantities on the lattice might exhibit larger τ_{int} . It can be shown in free field models that autocorrelation modes are related to lattice symmetries like *e.g.* translation invariance, and in this way to correlations on the lattice itself. As a consequence long range correlations across the lattice, as they occur for light masses, go along with larger autocorrelation times.

In the following we determine the autocorrelation from a variety of observables. This is facilitated because we have archived all trajectories

⁵Residual autocorrelation between successive measurements are taken into account by binning the data prior to statistical analysis [30].

of the SESAM-simulation and every second trajectory of the T χ L-simulation for a detailed post-processing.

We illustrate the numerical impact of finite sampling on the estimate of autocorrelation in Fig. 8. One observes the long range autocorrelation modes to emerge out of the noise level as the sample is enlarged. There is a certain threshold where the autocorrelation function ceases to be compatible with zero and becomes visible.

Besides the average plaquette S_\square , we computed the autocorrelation of extended smeared observables that exhibit a large ground state overlap per construction. This corresponds to rather long range correlations on the lattice. We consider the Gaussian smeared light meson masses, m_π and m_ρ , and smeared spatial Wilson and Polyakov loops built iteratively from fuzzed links of the form:

$$\begin{aligned} U_j^0(x) &= U_j(x) \\ U_j^{n+1}(x) &= U_j^n(x) U_j^n(x + 2^n \hat{j}) \\ &+ \sum_{|i| \neq j; i = \pm 1, \dots, 3} U_i^n(x) U_j^n(x + 2^n \hat{i}) \\ &\quad \times U_j^n(x + 2^n(\hat{i} + \hat{j})) \\ &\quad \times U_i^{n+1}(x + 2^{n+1} \hat{j}). \end{aligned} \quad (11)$$

n labels the smearing level. We investigate these quantities for $n = 0, 1, 2, 3$ corresponding to $1 \times 1, 2 \times 2, 4 \times 4, 8 \times 8$ Wilson loops, respectively.

Another ‘fermionic’ monitoring quantity is the inverse of the average number of iterations N_{kry}^{-1} of the Krylov solver. For the conjugate gradient (CG) it has been demonstrated in Ref. [31] that this quantity is related to the square root of the ratio of the minimal to the maximal eigenvalue of a hermitian positive definite matrix H , *i.e.*, its condition number $K = \frac{\lambda_{max}}{\lambda_{min}}$. This is motivated by the following considerations: let us start from the definition of κ_{sea}^c as the value of the hopping parameter, κ , at which the pion mass vanishes

$$m_\pi^2 \propto m_q = \frac{1}{2} \left(\frac{1}{\kappa} - \frac{1}{\kappa_{sea}^c} \right). \quad (12)$$

The convergence rate of the conjugate gradient algorithm, given a residual norm r , can be ex-

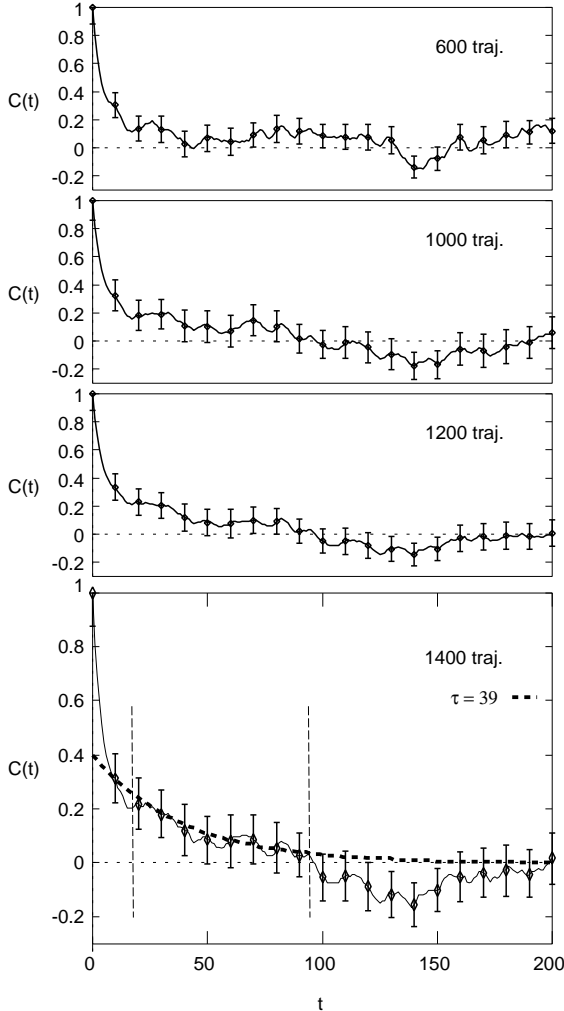


Figure 8. For $\kappa_{\text{sea}} = 0.157$, measurements on samples of increasing size are shown for the average plaquette.

tracted from the bound [32]

$$r \leq 2 \left(\frac{\sqrt{\lambda_{\max}} - \sqrt{\lambda_{\min}}}{\sqrt{\lambda_{\max}} + \sqrt{\lambda_{\min}}} \right)^{N_{CG}}. \quad (13)$$

This inequality provides an estimate to the convergence behaviour of CG on a hermitian matrix H . The relation is based on the assumption of a

uniform distribution of eigenvalues of H . Generally one expects some dependence of r on the detailed distribution of eigenvalues, however. Close to κ_c the minimal real eigenvalue of $M^\dagger M$ is small and is approximately that of M^2 , *i. e.*,

$$r \leq 2 - 4N_{CG} \frac{\lambda_{\min}}{\lambda_{\max}} + O \left[\left(\frac{\lambda_{\min}}{\lambda_{\max}} \right)^2 \right]. \quad (14)$$

For the case of a poor condition number, $\frac{\lambda_{\min}}{\lambda_{\max}} \ll 1$, we can exploit this relation and find for r fixed:

$$N_{CG}^{-1} = \lambda \propto \frac{\lambda_{\min}}{\lambda_{\max}}. \quad (15)$$

We know empirically that the ratios of convergence rates of BiCGstab and CG are quite constant over a rather large range of κ . This suggests to utilise the convergence rate of BiCGstab as an indicator to the Monte Carlo evolution of the smallest eigenvalue of the fermion matrix. Since small eigenvalues correspond to large correlation lengths, λ_{\min} presumably projects maximally onto the slowest relevant autocorrelation mode of the system.

In Fig. 9 the integrated autocorrelation times of sl and ss-smearing π and ρ ‘masses’ are shown. Here we take the ‘mass’ as computed from the propagator of each individual trajectory as an estimate. Autocorrelations of various gluonic observables (Wilson loops and Polyakov loops) are displayed in the lower part of the figure. In both pictures λ , as estimated by Eq. 15, is at the upper end for the autocorrelation times⁶, together with the 8×8 Wilson loop.

The plot illustrates the quality of the signal. It is evident that the exponential autocorrelation times are bounded by the minimal eigenvalue. For all reference quantities we observed clear plateaus in $\tau_{\text{int}}(t)$. The Wilson and Polyakov loops provide evidence that geometrically extended quantities indeed suffer more from autocorrelation effects.

So far, we have compared various observables at one value of κ_{sea} , $\kappa_{\text{sea}} = 0.157$. In the following

⁶Slower modes might exist for the topological charge, but seem to be decoupled from the observables of interest.

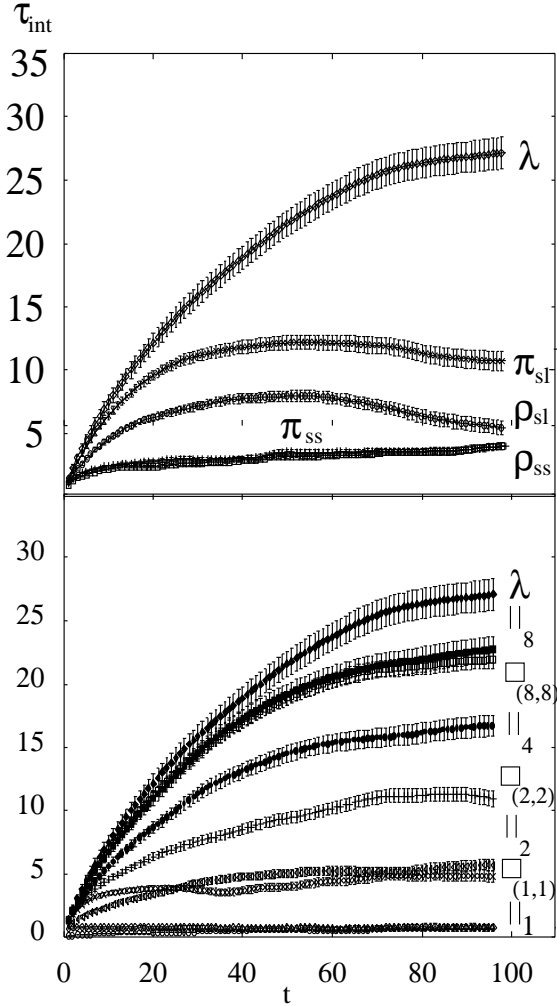


Figure 9. For $\kappa_{sea} = 0.157$, we demonstrate that the integrated autocorrelation time of λ is an upper bound for the autocorrelation times of all ‘fermionic’ and ‘gluonic’ observables measured.

Fig. 10, the sea-quark dependency of the exponential autocorrelation function is illustrated for three different observables: the plaquette action, the sl-smear pion mass and the spatial Wilson loop, $||_{(8,8)}$.

The smeared quantities exhibit an early asymptotic

behaviour while the un-smear average plaquette appears to couple to many excited modes. The *integrated* autocorrelation times, $\tau_{int}(t)$, of the pion masses and the spatial Wilson loops as a function of the cut-off t each reach an asymptotic plateau for $t_{int} < 1/4t$ within the estimated errors. Assuming a single exponential to dominate $\rho^A(t)$, the systematic error is $\approx 2\%$ and thus smaller than the statistical uncertainty.

A compilation of all integrated autocorrelation times can be found in Fig. 11

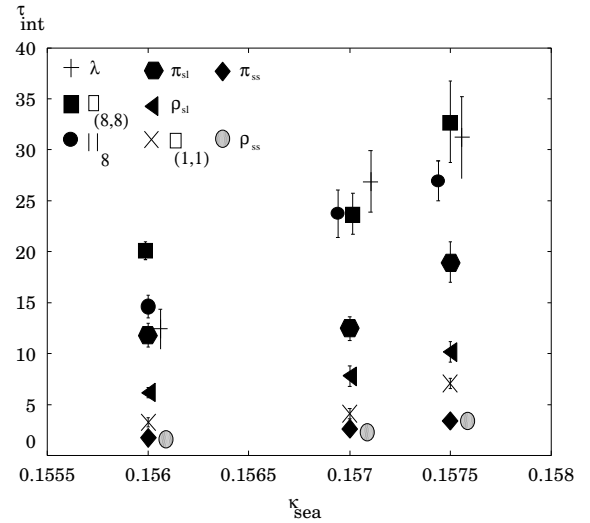


Figure 11. The sea quark-dependency of the estimated integrated autocorrelation times.

Originally we believed that the restriction of the pseudo-fermionic d.o.f. to the even sub-space [20], as offered by the o/e preconditioning scheme for M , would affect the dynamics of HMC only marginally, such that we have chosen this option. In the LL-SSOR scheme, however, the pseudo-fermion field has to live on the entire lattice.

It is now very interesting to compare autocorrelation on the full and the o/e reduced system, see Fig. 12: we show the integrated autocorrelation time of λ for $\kappa_{sea} = 0.1575$. On the fully

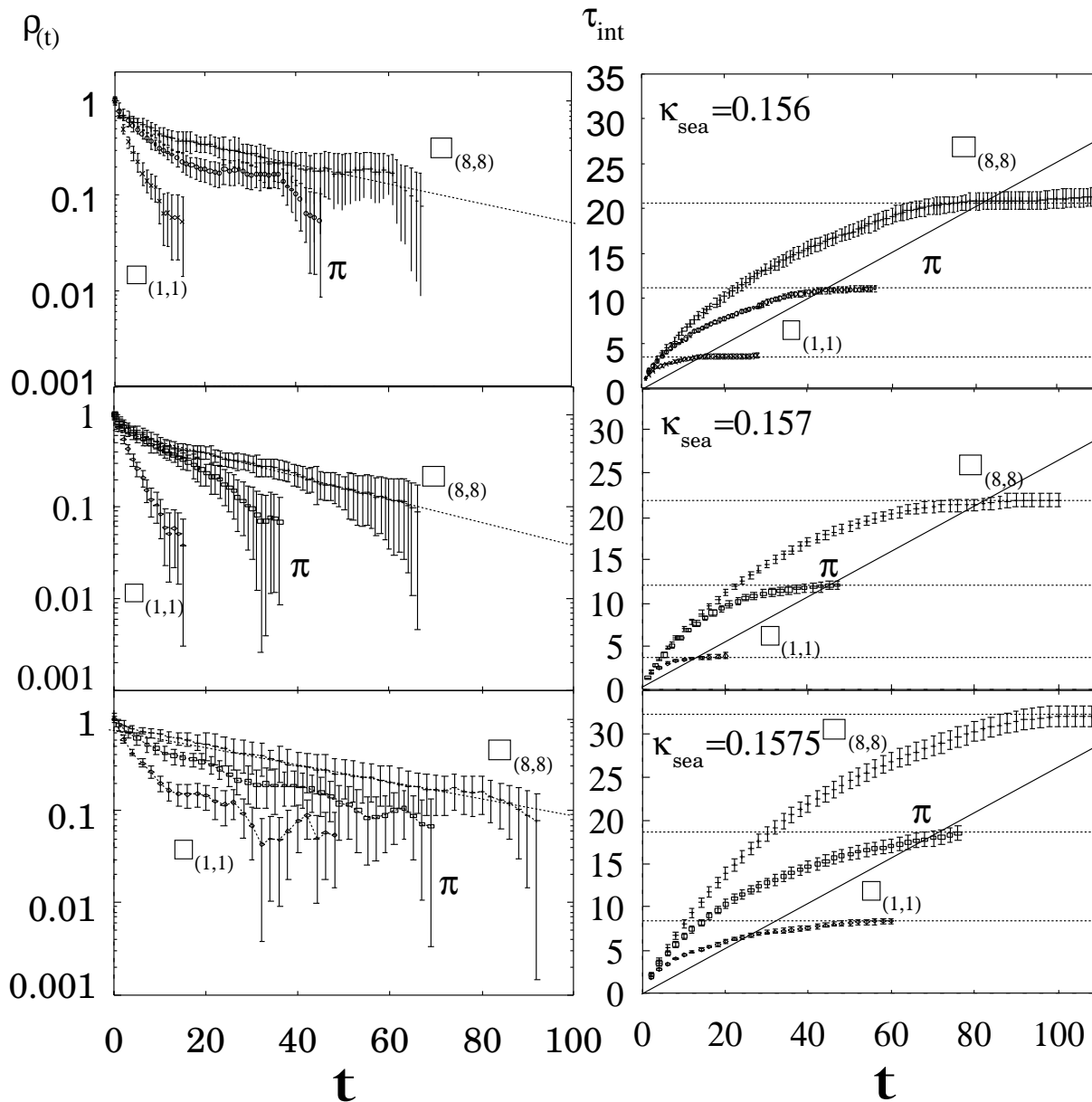


Figure 10. Autocorrelation functions and integrated autocorrelation times for the quantities: S_{\square} , π , $\square_{8,8}$ for all three sea quark masses. The 2% curve is plotted for orientation. The horizontal lines indicate the values of exponential and integrated autocorrelation times.

occupied system, we have employed the SSOR algorithm and have generated trajectories of half length, $T = 0.5$. One would have anticipated the autocorrelation time to increase by a factor of $\sqrt{2}$ in trajectories. We found, however, a factor of $\sqrt{2}$ only compared to the o/e reduced system's value. Thus, doubling the number of pseudo-fermionic degrees of freedom appears to affect autocorrelation to the extent that higher stochasticity decreases the autocorrelation.

The lessons to be learnt here are: the question of optimal trajectory length of the HMC has to be addressed anew and thinning out fermions turns out to be counter-productive.

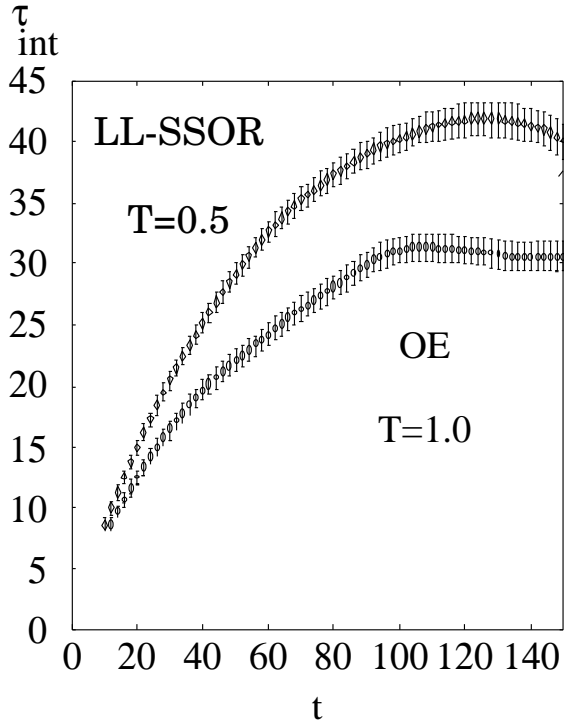


Figure 12. The integrated autocorrelation time of the averaged number of BiCGstab iterations for $\kappa_{\text{sea}} = 0.1575$.

For the algorithmic part of this talk we con-

clude that the autocorrelation times come out much smaller than anticipated previously. The exponential autocorrelation times all are well below the value of 50 trajectories. With the knowledge of τ_{int} , we can assess the computational cost to generate *one* independent full QCD vacuum state. Taking the sustained performances reached in the o/e and LL-SSOR preconditioned HMC (67% and 38%, respectively) we estimate these numbers in Gflops-hours units, see Tab. 4. More detailed results will be given in [33].

4. FLAVOUR SINGLET OPERATORS

The computation of nucleonic matrix elements of flavour singlet operators involves notorious noise problems when dealing with the contributions of disconnected quark diagrams (DQD). This presents a headache in particular, when analysing full QCD vacuum configurations for sea quark effects, given the limitations in the statistical sampling.

The common technique to handle DQD is the stochastic estimator method. SESAM has paid particular attention to devise methods for signal improvements, starting out from the work of the Tsukuba and Kentucky groups [27,26] in the quenched situation [28].

The most simple case of DQD to consider is the π -N σ -term, σ_N , which amounts to determine the correlator between the nucleon propagator, P , and disconnected closed quark loops, $Tr(M^{-1})$. According to the Kentucky technique the latter are estimated by inverting the Dirac operator on a stochastic source, with Z_2 noisy entries in all space-time and spin-colour components of the source vector.

The quantity to measure is given by the asymptotic slope in time t , in the expression for the correlator

$$\begin{aligned}
 R(t)^{disc} &= \frac{\langle P(0 \rightarrow t) Tr(M^{-1}) \rangle}{\langle P(0 \rightarrow t) \rangle} - \langle Tr(M^{-1}) \rangle \\
 &\xrightarrow{t \text{ large}} \text{const} + t \langle P|\bar{q}q|P \rangle_{disc}^{latt}, \quad (16)
 \end{aligned}$$

which is prone to noise problems from the very subtraction on the entire space-time volume. It

Table 4
CPU cost for the generation of full QCD vacuum states from our Quadrics implementation.

LATTICE $16^3 32$ at $\beta = 5.6$					
κ_{sea}	$a_\rho^{-1}[\text{GeV}]$	$L_S[\text{fm}]$	m_π	m_π/m_ρ -ratio	QH2[H] \rightarrow GFLOPS \times H
0.156 (OE)	2.19(8)	1.44(5)	0.4482(40)	0.8388(41)	$\approx 5 \rightarrow \approx 43$
0.157 (OE)	2.25(6)	1.39(4)	0.3412(33)	0.7552(69)	$\approx 22 \rightarrow \approx 189$
0.157 (SSOR)	"	"	"	"	$\approx 17 \rightarrow \approx 82$
0.1575 (OE)	2.38(7)	1.32(4)	0.2763(29)	0.688(12)	$\approx 45 \rightarrow \approx 387$
0.1575 (SSOR)	"	"	"	"	$\approx 35 \rightarrow \approx 170$

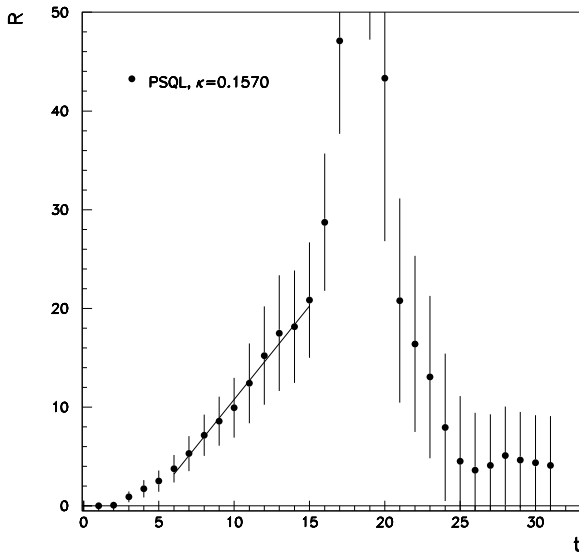


Figure 13. New plateau sampling technique for the computation of disconnected contributions to the π - N σ term in full QCD.

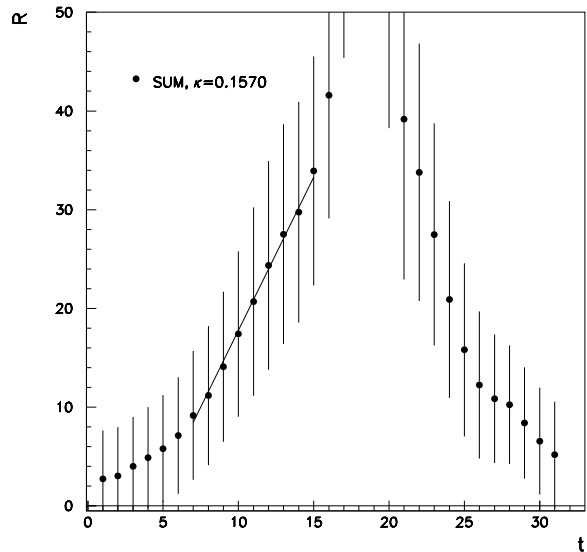


Figure 14. Same as Fig. 13. The source is spread over the entire lattice.

is obvious that loops located far away from $P(0 \rightarrow t)$ in time will add in particular to this noise level. But the highly separated terms (in time) are expected to be decorrelated from the nucleon propagator! The obvious measure to counteract the loss of signal is to confine the noisy source into the time interval of $0 < \tau < t$. This new *plateau sampling* technique leads to a substantial improvement of the signal to σ_N , as can be seen from Fig. 13. The variance turns out to be reduced by almost a factor 2, see Fig. 14.

This result is very encouraging in view of other, more complicated matrix elements, such as the

flavour singlet axial vector current which is of tantamount importance in proton spin studies. In this case a weak signal has been observed on a large quenched sample by the Tsukuba group some time ago [27]. The QCDSF collaboration, however, could not see a signal above the noise level, within their high statistics study of the proton structure functions [29]. It is a challenge to look for progress in the signal preparation.

5. LIGHT HADRONS SPECTRUM

With three SESAM samples at $\beta = 5.6$ (and one T χ L sample at $\kappa_{sea} = 0.1575$) we can perform the

chiral extrapolation in κ_{sea} for hadronic observables. We try to estimate the influence of dynamical fermions by comparison with quenched QCD at the equivalent scale. At each sea-quark sample zero-momentum two-point functions for mesons and baryons (*cf.* Tab. 5) are computed for various valence hopping parameters κ_V . Altogether

Table 5
Hadron operators.

meson	$\chi(x)$
pseudoscalar	$\chi_{PS}(x) = \bar{q}'(x)\gamma_5 q(x)$
vector	$\chi_V^\mu(x) = \bar{q}'(x)\gamma^\mu q(x)$
scalar	$\chi_{Sc}(x) = \bar{q}'(x)q(x)$
axial-vector	$\chi_{Ax}(x) = \bar{q}'(x)\gamma_5\gamma^\mu q(x)$
baryon	$\chi(x)$
nucleon	$\chi_N(x) = \epsilon_{abc}(q_a C \gamma_5 q_b) q_c$
Δ	$\chi_\Delta^\mu(x) = \epsilon_{abc}(q_a C \gamma^\mu q_b) q_c$

we work with fifteen mass estimates per κ_{sea} , see Tab. 6.

Table 6
Valence kappa values.

κ_{sea}	$\{\kappa_V\}$
0.156	{0.156, 0.157, 0.1575, 0.158, 0.1585}
0.157	{0.1555, 0, 156, 0, 1565, 0.157, 0.1575}
0.1575	{0.1555, 0, 156, 0, 1565, 0.157, 0.1575}

We want the propagators to be dominated by the lightest state at small time separations. Therefore we apply Wuppertal smearing with smearing parameter $\alpha = 4$ and 50 smearing iterations. Smear-smeared (ss) and smear-local (sl) correlators are used in simultaneous mass estimates. We fit to the data on time-slices 10 to 15 (see Ref. [30] on how to determine the fit ranges and all that). Autocorrelation times of $\tau_{\text{int}} < 25$ trajectories have suggested to calculate propagators on configurations separated by 25 HMC trajectories, the residual correlation is taken into account by jackknife binning.

We perform single-exponential fits:

$$\begin{aligned} C(t)_{\text{mes}} &= A(e^{-mt} + e^{-m(T-t)}), \\ C(t)_{\text{bar}} &= Ae^{-mt}. \end{aligned} \quad (17)$$

The effective masses are determined iteratively for the mesons, by solving the equation

$$\begin{aligned} &\frac{C_{AB}(t)}{C_{AB}(t+1)} \\ &= \frac{e^{-m_{\text{eff}}(t)t} + e^{-m_{\text{eff}}(t)(T-t)}}{e^{-m_{\text{eff}}(t)(t+1)} + e^{-m_{\text{eff}}(t)(T-t-1)}}, \end{aligned} \quad (18)$$

and directly for baryons,

$$m_{\text{eff}}(t) = \log \frac{C_{AB}(t)}{C_{AB}(t+1)}. \quad (19)$$

Light Mesons

We carry out linear extrapolations in the lattice quark mass, using data with $\kappa_V = \kappa_{\text{sea}}$, generically called m_{ss} :

$$\begin{aligned} m_{\text{PS,ss}}^2 &= c \left(\frac{1}{\kappa_{\text{sea}}} - \frac{1}{\kappa_{\text{sea}}^c} \right), \\ m_{V,ss} &= m^{\text{crit}} + bm_{\text{PS,ss}}^2. \end{aligned} \quad (20)$$

These fits, called ‘‘symmetric’’, are shown in Fig. 15. We find the pseudoscalar mass to be well matched by the linear ansatz (with a $\chi^2/\text{d.o.f} = 0.002$), whereas the vector masses may exhibit some downward curvature (based on a $\chi^2/\text{d.o.f} = 1.1$). The lattice spacing is obtained from M_ρ as physical input⁷. The results are quoted at both the chiral limit and the experimentally given mass ratio, defining $\kappa_{\text{sea}}^{\text{light}}$:

$$\frac{m_\pi}{m_\rho} = 0.1785. \quad (21)$$

The lattice spacings from the ρ become

$$\begin{aligned} a_\rho^{-1} &= 2.35(6) \text{ GeV} \quad \text{at } \kappa_{\text{sea}}^c, \\ a_\rho^{-1} &= 2.33(6) \text{ GeV} \quad \text{at } \kappa_{\text{sea}}^{\text{light}}, \end{aligned} \quad (22)$$

with

$$\kappa_{\text{sea}}^c = 0.15846(5), \quad \kappa_{\text{sea}}^{\text{light}} = 0.15841(5). \quad (23)$$

⁷Continuum masses go with capital ‘‘M’’, whereas lattice masses are written as ‘‘m’’.

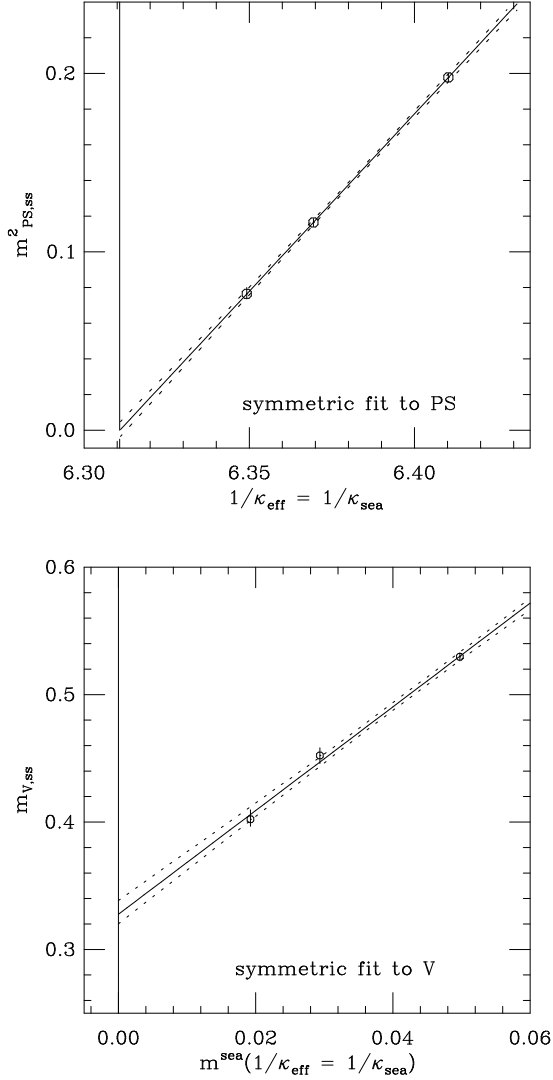


Figure 15. $m_{PS,ss}^2$ as a function of $\frac{1}{\kappa_{\text{sea}}}$ and $m_{V,ss}$ as a function of m^{sea} (in lattice units).

Strange Mesons

For want of 3 dynamical quarks, we have to find a way to compute strange mesons in a sea of two light mesons. This requires valence quarks different from sea quarks. We define an effective

κ through $\frac{1}{\kappa_{\text{V}}^{\text{eff}}} = \frac{1}{2} \left(\frac{1}{\kappa_{\text{V}}^1} + \frac{1}{\kappa_{\text{V}}^2} \right)$, where κ_{V}^1 and κ_{V}^2 refer to valence quarks in a meson.

In Ref. [34], we have introduced a notation to specify these valence quarks with masses different from sea quark masses. m_{ss} refers to both m^{V} 's equal m^{sea} of the sample, m_{sv} means only one m^{V} equal to m^{sea} , and m_{vv} stands for neither m^{V} equal to m^{sea} . We argued that $m_{PS,vv}^2$ and $m_{PS,sv}^2$ as linear functions of $\frac{1}{\kappa_{\text{sea}}}$ and $\frac{1}{\kappa_{\text{V}}}$ can be parametrised by the two sets of equations:

$$\begin{pmatrix} m_{PS,ss}^2 \\ m_{PS,sv}^2 \\ m_{PS,vv}^2 \end{pmatrix} = \begin{pmatrix} 2c & 0 \\ c + c_{13} & c - c_{13} \\ c_{34} & 2c - c_{34} \end{pmatrix} \begin{pmatrix} m^{\text{sea}} \\ m^{\text{V}} \end{pmatrix}, \quad (24)$$

$$\begin{pmatrix} m_{V,ss} \\ m_{V,sv} \\ m_{V,vv} \end{pmatrix} = m^{\text{crit}} + b \begin{pmatrix} m_{PS,ss}^2 \\ m_{PS,sv}^2 \\ m_{PS,vv}^2 \end{pmatrix}, \quad (25)$$

with $c_{34} = 2c_3$ and $c_{13} = 2c'_3 - c$ and $m^{\text{V}} = \frac{1}{2} \left(\frac{1}{\kappa_{\text{V}}^{\text{eff}}} - \frac{1}{\kappa_{\text{sea}}^c} \right)$. A combined linear fit of all the pseudoscalar data with the ansatz of Eq. 24 leads to an acceptable $\chi^2/\text{d.o.f} = 4.4/23$. For further details and the vector meson fits we refer to [30].

We determine κ^{strange} from m_{sv} by matching

$$\frac{m_{V,sv}(\kappa_{\text{sea}}^{\text{light}}, \kappa^{\text{strange}})}{m_{V,ss}(\kappa_{\text{sea}}^{\text{light}})} = \frac{M_{K^*}}{M_{\rho}} = 1.16, \quad (26)$$

where $\kappa_{\text{sea}}^{\text{light}}$ is given by Eq. 23. Alternatively, κ^{strange} is computed from m_{vv} matching

$$\frac{m_{V1,vv}(\kappa_{\text{sea}}^{\text{light}}, \kappa^{\text{strange}})}{m_{V2,ss}(\kappa_{\text{sea}}^{\text{light}})} = \frac{M_{\phi}}{M_{\rho}} = 1.326. \quad (27)$$

In this manner we can calculate the masses of the K (K^*) and the ϕ composed of the appropriate light and strange quarks in a sea of light quarks.

Baryon Masses

The remaining independent quantities to determine after fixing κ_{sea}^c via pseudoscalar meson mass and a via ρ mass are the masses of nucleon and Δ . We perform the chiral extrapolation by fitting to a linear function, the systematic error is taken from quadratic 3 parameter fits.

In Fig. 16 we show an overview of light and strange hadron masses comparing our three simulations (SESAM, T χ L, and quenched)⁸. π and ρ are used to fix scales and chiral limit and therefore must coincide with experimental values. For the Δ , sea quark effects seem to be visible, while for the nucleon there is no observable difference to quenched simulations. It remains to be seen how these findings are affected including the $\kappa = 0.158$ sample from T χ L. As expected finite volume effects (comparing extrapolations on SESAM data with T χ L data for $\kappa = 0.1575$) are largest for nucleon and Δ (around 5 to 8 %). The conversion to physical units slightly softens this effect since the ρ is some 2 to 3 % lighter on the 24^3 lattices. From the statistical accuracy achieved a sensible

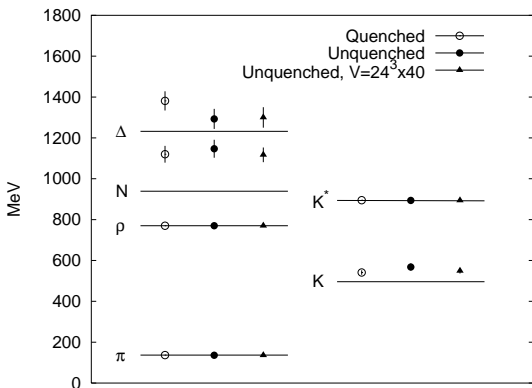


Figure 16. The light mass spectrum in the ‘simultaneous’ chiral limit.

continuum extrapolation appears to be in reach of Tera-computer performance!

⁸The T χ L data are preliminary ($\kappa = 0.1575$ only).

6. LIGHT QUARK MASSES

Light quark masses—albeit being fundamental parameters of the Standard Model—are not directly accessible to experiment.

In principle, lattice methods allow to compute their absolute values from the QCD Lagrangian, using the values of hadron masses as physical input [35–37]. Wilson fermions appear appropriate here as—unlike staggered fermions—they discretise full QCD with correct flavour attributes.

In a recent analysis of world data, unquenching (from $N_f = 0$ to $N_f = 2$) seems to lower the values of light and strange quark masses by about 50 % [37]. To clarify these indications we have investigated, within the SESAM project, the mass renormalization of the light and strange quarks under the influence of two dynamical flavors [34].

In order to extract the masses of the light and the strange quark from our meson data the lattice results have been extrapolated to the experimental mass ratios Eq. 21, Eq. 27, and Eq. 26. At each sea-quark sample we evaluate meson masses with strange valence quarks and perform an extrapolation of these masses to the physical sea of light quarks.

Under the condition that we have to treat the u - d isospin doublet as degenerate we can extract the masses of the degenerate light quarks in a sea of degenerate light quarks as well as the mass of the strange quark.

We take the values from our light spectrum computations and convert to physical units in the \overline{MS} -scheme according to:

$$m_{\overline{MS}}(\mu) = Z_M(\mu a) m^{\text{sea}} a_\rho^{-1}, \quad (28)$$

$Z_M(\mu a)$ is computed in boosted 1-loop perturbation theory [35,39]. Finally we run the values to 2 GeV, see Tab. 7.

We remark that one could have determined κ^{strange} by matching the ratio $\frac{M_\phi}{M_\rho}$ using the symmetric fit only [37], see Tab. 7. This result, $m_{\overline{MS}}^{\text{strange}}(2 \text{ GeV}) = 80(8) \text{ MeV}$ turns out to be much smaller than the value found before, $m_{\overline{MS}}^{\text{strange}}(2 \text{ GeV}) = 140(20) \text{ MeV}$. However, the ϕ would consist of strange valence quarks under the influence of a sea of strange quarks, which is a poor description of the physically correct situa-

Table 7

κ -values and corresponding light quark masses. The scale is taken from the ρ : $a_\rho^{-1}2.33(6)$ GeV at $\kappa_{\text{sea}}^{\text{light}}$.

	κ	$m_{\overline{MS}}(2 \text{ GeV})$
$N_f = 2$		
light	0.15841(5)	2.7(2) MeV
strange	0.15615(20) ^{stat} (20) ^{syst}	140(20) MeV
strange sea	0.15709(12)	80(8) MeV
$N_f = 0$		
light		5.5(5) MeV
strange		166(15) MeV

tion of two light dynamical quarks.

Comparing our results to the quenched values at corresponding $\beta_{\text{quenched}} = 6.0$, we observe a much smaller dynamical light quark mass [37]. $m^{\text{strange}}/m^{\text{light}} \approx 52$, whereas the strange mass is compatible to the quenched value within errors.

Let us comment on the dramatic change in the light quark mass due to unquenching. We can define a quark mass at *fixed* sea-quark:

$$m^{\text{V}} = \frac{1}{2} \left(\frac{1}{\kappa_{\text{eff}}^{\text{V}}} - \frac{1}{\kappa_{\text{V}}^{\text{c}}} \right). \quad (29)$$

Setting $m_{\text{PS},\text{w}}^2(\kappa_{\text{V}}^{\text{c}}) = 0$ at $\kappa_{\text{V}}^{\text{c}} \neq \kappa_{\text{sea}}^{\text{c}}$ forces the ‘pion’ to become massless at $\kappa_{\text{V}}^{\text{c}}$.

In the manner of quenched computations we measure a ‘bare light quark mass’ at each of the three sea-quark values. A chiral extrapolation of these quark masses in the sea-quark to the chiral point would yield the value Δ_2 in Fig. 17, while the true value (from a pion at a physical sea-quark) is given by $\Delta_1 < \Delta_2$. We might try to solve this Δ_1 - Δ_2 -discrepancy and extrapolate Δ_2 to the location of the light sea-quarks. However, either we give up working at the physical pion mass—as the critical kappa $\frac{1}{\kappa_{\text{V}}^{\text{c}}}$ would become too low otherwise—or again the ‘quark mass’ given in this way is too large by about a factor 2. As these ‘light quark masses’ are very similar to that of the quenched simulation (5.7(4), 5.6(3), 5.4(3) MeV), the conclusion is that it is not possible to estimate the light quark mass from quenched computations since the light quark mass known by symmetric extrapolation cannot be recovered computing in valence quark style at fixed sea quark mass, with subsequent extrapolation in m^{sea} .

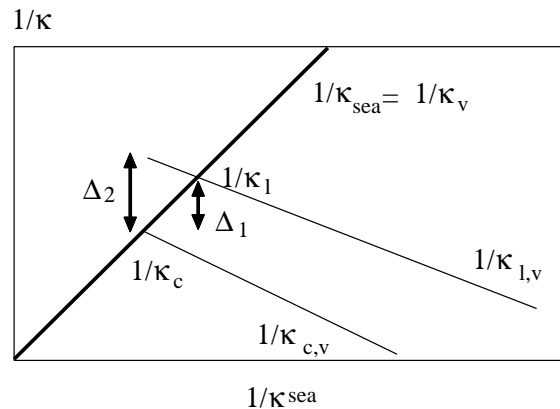


Figure 17. Schematical plot of $\frac{1}{\kappa_{\text{V}}^{\text{c}}}$ and $\frac{1}{\kappa_{\text{V}}^{\text{light}}}$ vs. $\frac{1}{\kappa_{\text{sea}}}$.

7. HEAVY QUARKONIA

As has been reported by C. Davies in her contribution to this workshop, nonrelativistic QCD (NRQCD), an effective theory for the low energy regime of heavy quarkonia, has proven to be an efficient tool to directly calculate bottomonium on the lattice [40]. Full QCD simulations using dynamical staggered quarks have shown the sensitivity of fine and hyperfine splittings to vacuum polarisation. Lattice observables extrapolated to $N_f = 3$ have turned out to be in remarkable agreement with experimentally known quantities, thus unknown quantities can be predicted with

some confidence.

In this section, we present preliminary results of our systematic study of lattice NRQCD for $b\bar{b}$ systems with dynamical Wilson quarks at three different masses, an NRQCD action that includes relativistic corrections of order $\mathcal{O}(M_b v^6)$, mean field improvement with u_0 computed from the mean link in Landau gauge and efficient wave function smearing.

7.1. Technique of NRQCD

The nonrelativistic Lagrangian is decomposed into the kinetic energy operator,

$$H_0 = -\frac{\Delta^{(2)}}{2M_b}, \quad (30)$$

which is of order $M_b v^2$, and relativistic corrections the importance of which is estimated via power counting. We include operators of order $M_b v^4$ and $M_b v^6$ [41],

$$\delta H = \delta H^{(4)} + \delta H^{(6)}, \quad (31)$$

with

$$\begin{aligned} \delta H^{(4)} = & \\ & - c_1 \frac{(\Delta^{(2)})^2}{8M_b^3} \\ & + c_2 \frac{ig}{8M_b^2} (\Delta \cdot E - E \cdot \Delta) \\ & - c_3 \frac{g}{8M_b^2} \sigma \cdot (\tilde{\Delta} \times \tilde{\mathbf{E}} - \tilde{\mathbf{E}} \times \tilde{\Delta}) \\ & - c_4 \frac{g}{2M_b} \sigma \cdot \tilde{\mathbf{B}} \\ & - c_5 \frac{a^2 \Delta^{(4)}}{24M_b} - c_6 \frac{a (\Delta^{(2)})^2}{16nM_b^2}, \end{aligned} \quad (32)$$

and

$$\begin{aligned} \delta H^{(6)} = & -c_7 \frac{g}{8M_b^3} \{\Delta^{(2)}, \sigma \cdot \mathbf{B}\} \\ & -c_8 \frac{3g}{64M_b^4} \{\Delta^{(2)}, \sigma \cdot (\Delta \times \mathbf{E} - \mathbf{E} \times \Delta)\} \\ & -c_9 \frac{ig^2}{8M_b^3} \sigma \cdot \mathbf{E} \times \mathbf{E}. \end{aligned} \quad (33)$$

Derivatives and fields with tilde have their leading order discretisation errors removed in order to

correct for $\mathcal{O}(a^2 M_b v^4)$ errors. Following Ref. [40] the quark Green's function is calculated from the evolution equation

$$\begin{aligned} G(t+1) &= \left(1 - \frac{aH_0}{2n}\right) U_4^\dagger \left(1 - \frac{aH_0}{2n}\right)^n \\ &\quad \times (1 - a\delta H) G(t), \quad (34) \\ G(0) &= \delta_{\mathbf{x},0}. \quad (35) \end{aligned}$$

The parameter n allows to stabilise the evolution in case of small bare quark masses. For the Υ system $n = 2$ is appropriate. The Lagrangian is tadpole improved a fact that may justify a tree level matching to QCD, i.e. all the coefficients c_i are set to one. Note, however, that first order perturbative corrections to some interactions may well be of the same sizes as relativistic $\mathcal{O}(M_b v^6)$ corrections. We choose u_0 to be the mean link in Landau gauge as recently there have been hints for better scaling properties associated with this choice compared to the average plaquette prescription [42]. We find a two percent difference in u_0 between both choices for all κ values. The tadpole improved chromo-fields then differ by about eight percent. Through the whole simulation we fix the heavy quark mass to a value $aM_b = 1.7$. Taking advantage of the smallness of the bottomonium system, we exploit configurations more than once by starting the propagator evolution both at different spatial source points located on one and the same timeslice and on different timeslices.

Meson correlation functions are built from quark propagators combined with suitable interpolating operators:

$$G_{\text{sc,sk}}^{\text{meson}}(t) = \sum_{\mathbf{x}, \mathbf{y}} \text{Tr} \left[G^\dagger(\mathbf{x}, t) \Gamma_{(sk)}^\dagger(\mathbf{y} - \mathbf{x}) \tilde{G}(\mathbf{y}, t) \right], \quad (36)$$

where the source smeared propagator \tilde{G} is obtained by evolving the extended source:

$$\tilde{G}(\mathbf{y}) = \sum_{\mathbf{x}} G(\mathbf{y} - \mathbf{x}, t) \Gamma_{(sc)}(\mathbf{x}). \quad (37)$$

We adopt spectroscopic notation and denote (radially excited) spin-parity eigenstates by $n^{2S+1}L_J$. The interpolating operator

$\Gamma^{(sc/sk)}(\mathbf{x}) \equiv \Omega\Phi^{(sc/sk)}(\mathbf{x})$ contains a spin matrix and a spatial smearing function. The latter is calculated as the solution of the Schrödinger Equation with the Cornell potential for definite radial quantum number and angular momentum. Note that 'local' P-states are realized through derivatives acting on the delta function. For the Υ and η_b we calculate a 4×4 matrix of correlations with $sc/sk = l, 1, 2, 3$ corresponding to a point source, the ground state, the first and second excited states respectively. For the $L = 1$ states we restrict ourselves to the ground state and the first excitation as signals are worse. Gauge configurations are fixed to Coulomb gauge.

7.2. Data Analysis

Figure 18 gives an impression of the signals' quality. Concerning the $L = 0$ states we are able to force correlators to stay in the first excitation for about ten time-steps. Local masses for P states are much noisier and drop to the ground state without dwelling in an 'excited plateau' first. To extract energies we fit several correlators simultaneously to a multi-exponential ansatz. We find that vector fits to smeared-local propagators,

$$G_{\text{meson}}^{(sc,l)}(t) = \sum_{k=1}^{n_{exp}} b_{sc,k} e^{-E_k t}, \quad (38)$$

are quite stable whereas matrix fits demand for higher statistics. Tab. 8 gives a representative sample of fits. We determine hyperfine splittings by single exponential fits to the ratio of smeared-local propagators thus exploiting the strong correlation between them. More complicated fit-functions confirm the results obtained from the single exponential ansatz but do not behave very stable.

7.3. Results

The lattice scale is taken from the average of the $2S - 1S$ and $CG(^3P) - 1S$ splittings (see Tab. 9). We do not include $\mathcal{O}(a^2)$ gluonic corrections at this stage as their effect is not visible with present statistic. For the ratio of splittings, $R = (2^3S_1 - 1^3S_1)/(CG(^3P) - 1^3S_1)$, we obtain a value $R = 1.28(10)$ at $\kappa = 0.1575$ and $R = 1.30(9)$ at $\kappa = 0.157$ which is consistent with the experimental number $R = 1.28$. Tab. 10 lists

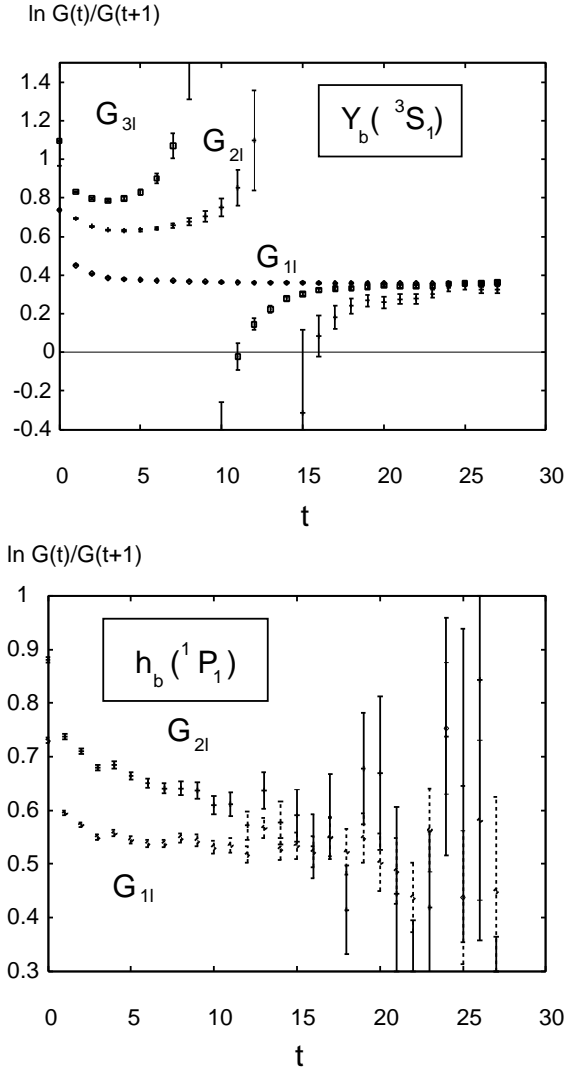


Figure 18. Effective masses of smeared-local correlators for the Υ and h_b , $\kappa_{sea} = 0.1575$, $n_{config} = 700$. Propagator indices label the radial quantum number of the smearing function. Note that G_{2l} and G_{3l} rise sharply indicating the sudden decay of the dominating excited state to the ground state.

Table 8

Vector Fits to smeared-local correlators for Υ and h_b states. Errors are calculated from 200 bootstraps.

N_{exp}	t_{min}	t_{max}	aE_1	aE_2	aE_3	χ^2/dof	Q
3S_1							
2	4	30	0.3589(8)	0.605(6)	—	54.5/48	0.241
	6	30	0.3587(8)	0.599(7)	—	46.9/44	0.355
	8	30	0.3586(8)	0.599(10)	—	46.1/40	0.235
	10	30	0.3583(9)	0.585(15)	—	44.1/36	0.167
3	4	25	0.3578(9)	0.589(12)	0.782(18)	63.0/54	0.188
	5	25	0.3581(10)	0.592(13)	0.762(28)	61.2/51	0.155
	6	25	0.3577(12)	0.574(18)	0.741(32)	58.2/48	0.148
	7	25	0.3579(11)	0.581(20)	0.78(5)	56.0/45	0.126
1P_1							
2	4	30	0.533(5)	0.728(20)	—	48.4/48	0.457
	5	30	0.535(6)	0.724(15)	—	41.2/46	0.672
	6	30	0.536(8)	0.719(21)	—	41.1/44	0.597
	7	30	0.533(10)	0.713(28)	—	40.6/42	0.534

our results in lattice units, Figure 19 sketches the Υ spectrum and hyperfine-splittings.

Table 9

Lattice Spacings.

Lattice Spacings	$\kappa=0.157$	$\kappa=0.1575$
$a^{-1}(2^3S_1 - 1^3S_1)[GeV]$	2.34(15)	2.48(14)
$a^{-1}(1^3S_1 - 1CG(^3P))[GeV]$	2.40(13)	2.50(11)

Table 10

Fit results for radial and spin splittings.

$aM_b^0 = 1.7$	$\kappa = 0.157$	$\kappa = 0.1575$
$2^1S_0 - 1^1S_0$	0.245(8)	0.240(7)
$3^1S_0 - 1^1S_0$	0.46(5)	0.41(4)
$2^3S_1 - 1^3S_1$	0.241(13)	0.226(15)
$3^3S_1 - 1^3S_1$	0.41(2)	0.38(3)
$1^1P_1 - 1^3S_1$	0.186(8)	0.176(9)
$2^1P_1 - 1^1P_1$	0.23(2)	0.18(3)
$1^3S_1 - 1^1S_0$	0.0142(2)	0.0135(2)
$1^3P_2 - 1^1P_1$	0.0032(11)	0.0039(5)
$1^1P_1 - 1^3P_1$	0.0040(10)	0.0026(7)
$1^1P_1 - 1^3P_0$	0.015(4)	0.013(2)

7.4. Remarks

We have presented preliminary results on the bottomonium spectrum calculated from NRQCD, in a gauge field background with 2 flavours of dynamical Wilson quarks. Radial excitations and hyperfine splittings have been determined for two ensembles of configurations corresponding to two different sea-quark masses. We observe better agreement with experiment as compared to the quenched result confirming the results of simulations with staggered fermions. Up to now we are, however, not able to give a conclusive statement concerning the dependence of energy levels on the dynamical quark mass. To decide on this issue and to disentangle unquenching effects from relativistic corrections we are going (i) to complete the analysis with a third κ -value ($\kappa_{sea} = 0.156$), (ii) we will carry out a quenched simulation for our choice of heavy quark action and (iii) we will exploit T χ L configurations at $\kappa_{sea} = 0.158$.

SUMMARY

I have tried to give an impression of the goals and achievements of the SESAM and the T χ L projects, simulations with Wilson fermions at intermediate lattice sizes and dynamical quark masses. To set a significant landmark we have concentrated on one β value.

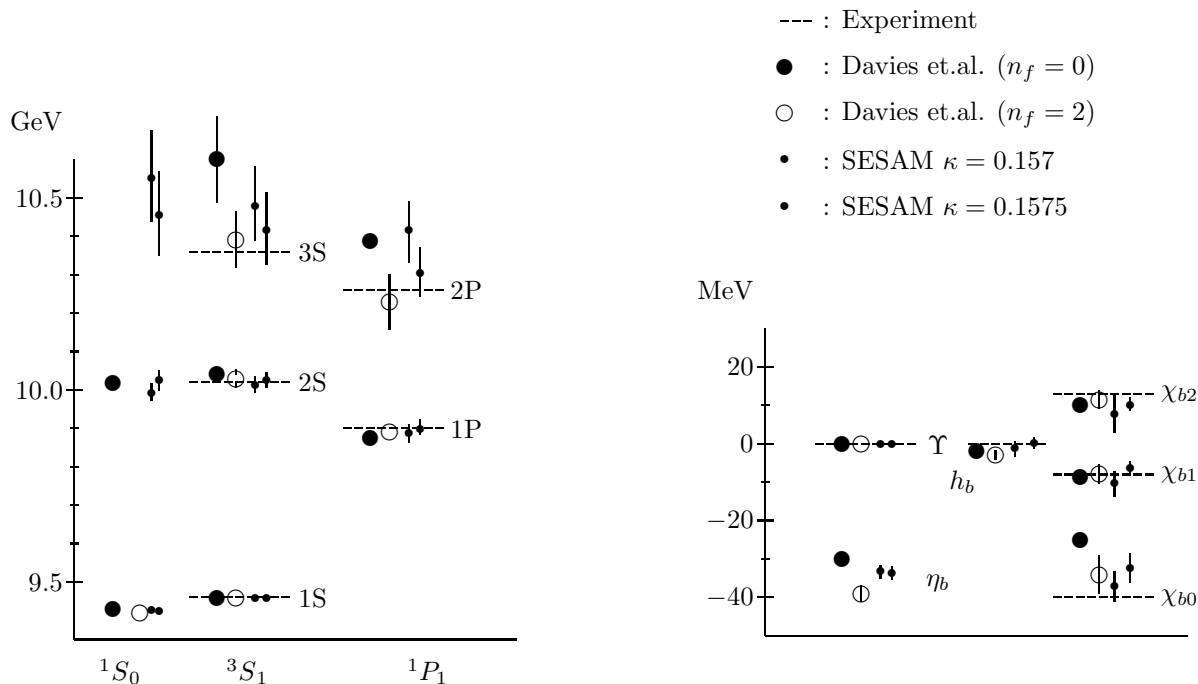


Figure 19. Υ Spectrum and Hyperfine Splittings: Quenched: $\beta = 6.0, 16^3 \times 32$ [40]; Dynamical Staggered: $\beta = 5.6, am_q = 0.01, 16^3 \times 32$ [43]; Dynamical Wilson: $\beta = 5.6, \kappa = 0.157, 0.1575, 16^3 \times 32$. Errors are purely statistical. Note that Davies et al. have updated their quenched simulation meanwhile, see C. Davies, these proceedings.

It would of course be highly desirable to carry out a scaling analysis in full QCD, *i.e.*, the extrapolation to the continuum limit. Such a study, making use of improved actions, will be the adequate computational challenge for computers of \geq CP-PACS performance!

Acknowledgments. We are indebted to Prof. A. Frommer and his group for a very pleasant and fruitful cooperation. Th. L. and K. S. thank Profs. Y. Iwasaki and A. Ukawa for their hospitality and a beautiful workshop at Tsukuba Center for Computational Physics. The work of Th. L. is supported by the Deutsche Forschungsgemeinschaft DFG under grant No. Schi 257/5-1.

REFERENCES

1. S. Duane, A. Kennedy, B. Pendleton and D. Roweth, Phys. Lett. B **195** (1987) 216.
2. S. Gottlieb et al., Phys. Rev. D **35** (1987) 2531.
3. R. Gupta, et al., Phys. Rev. D **44** (1991) 3272.
4. K.M. Bitar et al, Nucl. Phys. **B** (Proc. Suppl.)**42** (1995)796.
5. K. M. Bitar et al., Phys. Rev. **D49** (1994) 3546.
6. K.M. Bitar, R.G. Edwards, U.M. Heller, A.D. Kennedy, Nucl. Phys. **B** (Proc. Suppl.) **53** (1997) 225-227.
7. SESAM-Collaboration: U. Glässner, S. Güsken, H. Hoerber, Th. Lippert, X. Luo, G. Ritzenhöfer K. Schilling and G. Siegert, in T. D. Kieu, B. H. J. McKellar, and A. J. Guttmann, (eds.): Proc. of *Lattice '95*, Nucl. Phys. **B** (Proc. Suppl.) **47** (1996) 386-393.
8. T χ L-collaboration, L. Conti, N. Eicker, L. Giusti, U. Glässner, S. Güsken, H. Hoerber,

- P. Lacock, Th. Lippert, G. Martinelli, F. Rapuano, G. Ritzenhöfer, K. Schilling, G. Siegert, A. Spitz, J. Viehoff, Nucl. Phys. B **53**, Proc. Suppl. (1997) 222-224.
9. S. Fischer, A. Frommer, U. Glässner, Th. Lippert, G. Ritzenhöfer, K. Schilling, Comp. Phys. Comm. **98** (1996) 20-34.
 10. S. Fischer, A. Frommer, U. Glässner, S. Güsken, H. Hoerber, Th. Lippert, G. Ritzenhöfer, K. Schilling, G. Siegert, A. Spitz, in C. Bernard, M. Golterman, M. Ogilvie, and J. Potvin, (eds.): Proc. of *Lattice '96*, Nucl. Phys. B (Proc. Suppl.), **53** (1997) 990-992.
 11. R. Kenway, these proceedings.
 12. A. Frommer, V. Hannemann, Th. Lippert, B. Nöckel, and K. Schilling, Int. J. Mod. Phys. C **5** (1994) 1073.
 13. A. Frommer, S. Güsken, Th. Lippert, B. Nöckel, K. Schilling, Int.J.Mod.Phys. C **6** (1995) 627-638.
 14. A. Frommer, in C. Bernard, M. Golterman, M. Ogilvie, and Jean Potvin, (eds.): Proceedings of *Lattice '96*, Nucl. Phys. B (Proc. Suppl.), **53** (1997) 120-126.
 15. R. Gupta et al., Phys. Rev. D **40** 2072 (1989).
 16. R. Freund, N. Nachtigal, Numer. Math. **60**, 315-339 (1991).
 17. H. van der Vorst, SIAM J. Sc. Stat. Comp. **13** (1992) 631-644.
 18. U. Glässner et al., hep-lat/9605008.
 19. Y. Saad and M. Schultz, SIAM J. Sc. Stat. Comp. **7** (1986) 856.
 20. T. DeGrand and P. Rossi, Comp. Phys. Comm. **60** 211 (1990).
 21. Y. Oyanagi, Comp. Phys. Comm. **42** (1986) 333.
 22. S. Eisenstat, SIAM J. Sci. Stat. Comput. **2** (1981) 1.
 23. G. Hockney, Nucl. Phys. B (Proc. Suppl.) **17** (1990) 301.
 24. R. C. Brower, T. Ivanenko, A. R. Levi, K. N. Orginos, Nucl. Phys. B **484** (1997) 353-374.
 25. A. D. Sokal, in Foundations and New Algorithms, Cours de Troisième Cycle de la Physique en Suisse Romande.
 26. S.J. Dong and K.F. Liu, Nucl.Phys. B (Proc.Suppl.) **26**(1992)353; Phys. Lett. B **328** (1994) 130, S.J. Dong and K.F. Liu, Nucl.Phys. B (Proc.Suppl.) **26** (1993) 487, K. F. Liu, S. J. Dong, T. Draper and W. Wilcox, Phys. Rev. Lett. **74**(1995)2172, S. J. Dong, J. F. Lagaë, and K.F. Liu, Phys. Rev. Lett. **75** (1995) 2096.
 27. Y. Kuramashi, M. Fukugita, H. Mino, M. Okawa, and A. Ukawa, Phys. Rev. Lett. **75** (1995) 2092, Phys. Rev. D **51** (1995) 5319.
 28. SESAM Collaboration: N. Eicker et al., Phys.Lett. B **389** (1996) 720-726.
 29. G. Schierholz, private communication.
 30. SESAM-collaboration, 'Hadron Spectrum in full QCD with two flavors of dynamial Wilson Fermions', in preparation.
 31. By I. Barbour, E. Laermann, T. Lippert, K. Schilling, Phys. Rev. D **46** (1992) 3618-3629.
 32. M. Engeli et. al., *Mitteilungen aus dem Institut für angewandte Mathematik* (Birkhäuser Verlag, Berlin, 1959), Vol. 8, S. 79ff.
 33. SESAM-collaboration, 'Critical Dynamics of the Hybrid Monte Carlo', in preparation.
 34. N. Eicker, U. Glässner, S. Güsken, H. Hoerber, P. Lacock, Th. Lippert, G. Ritzenhöfer, K. Schilling, G. Siegert, A. Spitz, P. Ueberholz, J. Viehoff (SESAM-Collaboration), hep-lat/9704019, acc. for publ. in Phys. Lett. B.
 35. C. R. Allton et al., Nucl. Phys. B **431** (1994) 667, C. R. Allton, V. Gimenez, L. Giusti and F. Rapuano, Nucl.hys. B **489** (1997) 427-452.
 36. B. J. Gough et al., Fermilab-Pub-96-283, hep-ph/9610223; see also P. B. Mackenzie, Nucl. Phys. Proc. Suppl. **53** (1997), 23.
 37. R. Gupta and T. Bhattacharya, hep-lat/9605039, Phys. Rev. D, to appear.
 38. T. Bhattacharya, R. Gupta and K. Maltman, hep-ph/9703455.
 39. G. P. Lepage and P. B. Mackenzie, Phys. Rev. D **48** (1993) 2250.
 40. C. T. H. Davies, K. Hornbostel, A. Langnau, G. P. Lepage, A. Lidsey, J. Shigemitsu, J. Sloan, Phys. Rev. D **50** (1994) 6963.
 41. G. P. Lepage, L. Magnea, C. Nakhleh, U. Magnea, K. Hornbostel, Phys. Rev. D **46** (1992) 4052.
 42. H. D. Trottier, hep-lat/9611026.
 43. P. McCallum et al., Nucl. Phys. B (Proc. Suppl.) **47** (1996) 409.